Supplemental Material and Methods

In vitro doxycycline and thrombin treatment

Cells were plated at 60% confluence in complete medium for 24 hours and treated ± 1 μg/ml doxycycline hyclate (Sigma, D3447) in RPMI 1640, 1% FBS medium for 24 hrs. Cells were then stimulated with 1 U/ml thrombin (Enzyme Research Lab, BT-1002a) for 1 hour and harvested for immunofluorescence, protein, or RNA analyses.

Immunoblotting

Immunoblotting was performed as previously described (19). Membranes were probed with primary antibodies for p-Erk 1:1000 (Cell Signaling, 9102), total Erk 1:1000 (Cell Signaling, 4377s), and Hsp90 1:5000 (Santa Cruz, SC-7947).

Histology, immunohistochemistry and immunofluorescence staining

Pancreas tissue or tumors were processed by formalin fixation, processing into paraffin, and sectioning onto slides. For immunohistochemistry staining, primary antibodies were applied to the slides for 1 hour at room temperature for TF (1:200, Abcam, 211016) and K19 (1:100, Dev. Studies Hybridoma Bank, troma3) or 4^{o}C overnight for PAR-1 (1:100, BD Transduction Laboratories 611523), phospho-H3 (1:1000, Millipore sigma 06570), cleaved caspase-3 (1:1000, Cell Signaling, D175), Iba-1 (1:1000, FUJIFILM Wako Pure Chemical Corporation, 016-20001), CD3 (1:100, Abcam 16669), CD31 (1:20, Dianova, SZ31), Arg1 (1:200, Abcam 91279), or iNOS (1:100, ThermoFisher, PA1-036). For immunofluorescence staining, anti-Myc (1:500, Santa Cruz, SC-40) and avidin-conjugated Alexa Fluor 594 (1:100, Invitrogen, S11227) were used. The area of staining was quantified using ImageJ or by counting the number of events per high powered field (HPF).

RT-qPCR

RNA was extracted and harvested using the E.Z.N.A. Total RNA kit (OMEGA, R6834-02). RNA was converted to cDNA using the iScript cDNA synthesis kit (Bio-Red, 1708891). Quantitative RT-PCR was performed with SYBR green (Roche, 04913850001) to establish relative transcript levels of each gene. All transcript levels were normalized to internal control *18S* expression using the ΔΔCT method to determine the relative fold change. Primer sequences for mouse *Par* and *TF* transcripts are as follows: *Par-1*: F-5'-ccagccagaatcagagaggac; R-5'-agtagactgccctaccctcc; *Par-2*: F-5' ctgggaggtatcacccttctg; R-5'-gagaactcatcgatggaaaagc; *Par-3*: F-5'-tttccacttgctgctcatacat; R-5' agttaaggttggctttgctgag; *Par-4*: F-5'-ctgctgtatcctttcgtgctg; R-5' actgtcgttggcacagaattt; *TF*: F-5'-acaattttggagtggcaacc; R-5'-tcacgatctcgtctgtgagg.

Cell proliferation assay

Cell growth rates were determined by the CyQUANT cell proliferation assay per manufacturer's instructions (Thermo Fisher, C7026). Doubling time was calculated as Duration * log(2)/log(final fluorescence) - log(initial fluorescence) using the log phase time points.

RNA-Seq and Bioinformatics

KPC2 and KPC2-Par1^{KO} cells were plated at 1x10^{6} cells per 6 cm dish in complete media. The following day cells were washed and placed in low serum (1% FBS) media for 24h. Cells were then dosed with 1U/mL thrombin or vehicle and RNA was harvested 24h post-treatment using a miRNeasy kit (Qiagen, 217004). Total RNA was submitted to the Purdue Genomics Core Facility for quality assessment and next-generation sequencing. Paired-end 2x100 bp sequencing was performed using a HiSeq2500 system (Illumina). Raw data are available through the NCBI Gene Expression Omnibus (GEO) database (accession number GSE120370). Reads were trimmed using the FastX-Toolkit with a minimum quality score of 30, leaving ~35M trimmed reads/sample. Trimmed reads were aligned to mouse genome (mm10) using Tophat2, and gene counts were obtained using HTSeq. Differential gene expression was determined using edgeR with an exclusion of genes having fewer than 0.5 counts per million (cpm) from the analysis. Differential genes were defined as those with a false discovery rate (FDR) ≤ 0.01 and a fold

change ≥ 2. Mouse Genome Informatics (MGI) phenotype enrichment was determined using WebGestalt.

Supplemental Figures

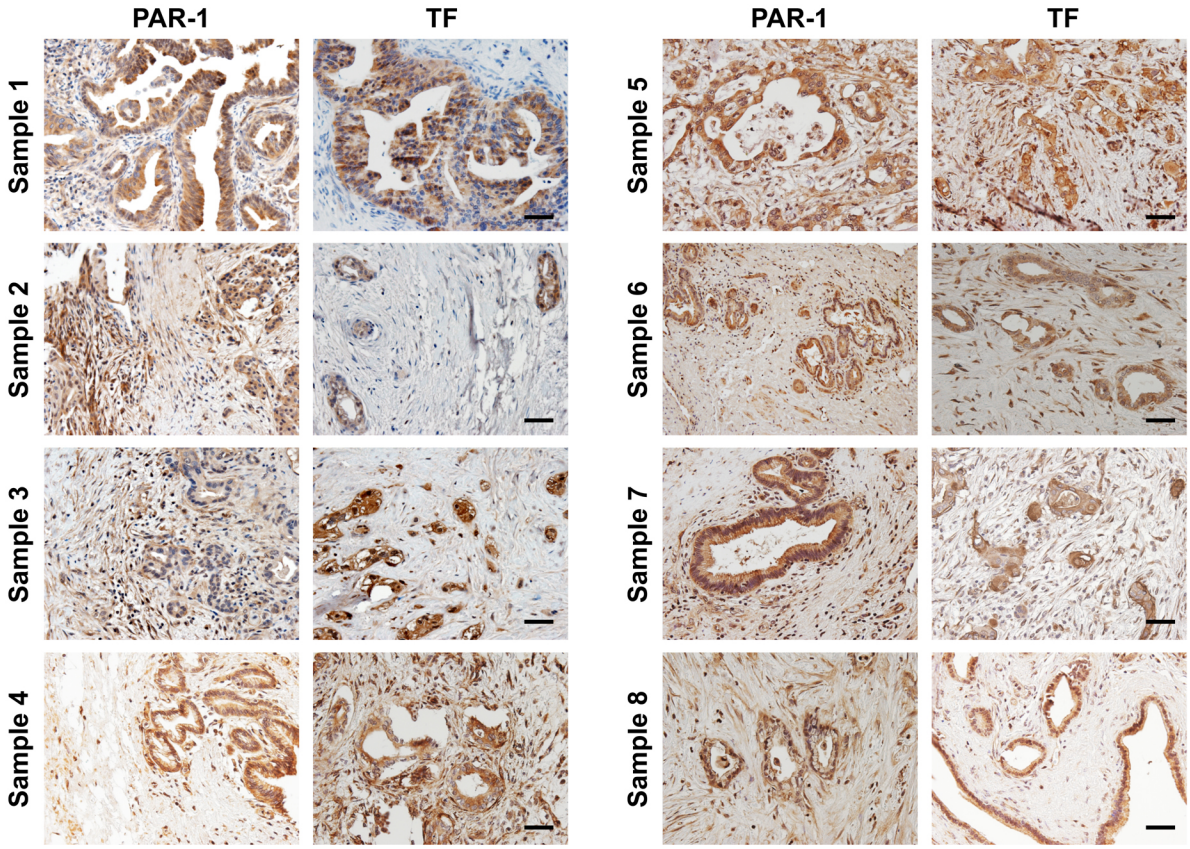

FIGURE S1: *Immunohistochemistry of PAR-1 and TF localization in PDAC patient biopsies.* Staining for PAR-1 and TF in eight independent PDAC tumor samples. In each case, high levels of PAR-1 are observed in 7 out of 8 PDAC tumor epithelial lesions and strong TF expression is observed in all PDAC epithelial lesions. Scale bars: 50 μm.

A

Summary of online data for increased TF expression in PDAC

Online Resource	Data Set	Increased Expression-Fold Change in PDAC	*P-value*
Oncomine	Ramaswamy Multi-cancer	9.062	8.94E-09
	Bittner Multi-cancer	4.287	3.74E-06
	Su Multi-cancer	6.504	8.13E-06
	Wagner CellLine	8.403	2.82E-06
	Garnett CellLine	8.881	2.90E-06
	Barretina CellLine	6.857	9.24E-12
	Badea Pancreas	2.725	2.96E-10
	Sagara Pancreas	3.177	4.00E-03
Human Protein Atlas	Expression in normal tissue = Low Expression in PDAC: 10/12 samples = Medium or High		

B

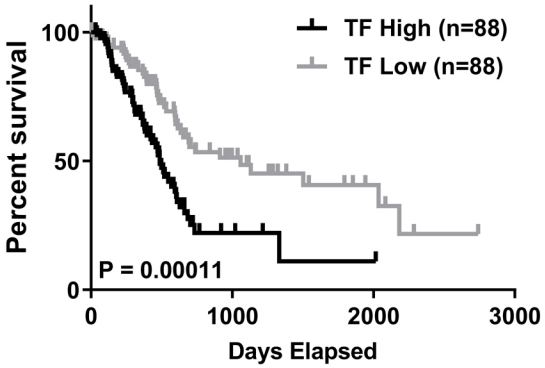

FIGURE S2: *Tissue factor is highly expressed in PDAC and increased expression of tissue factor is linked to poor PDAC patient prognosis.* **(A)** A summary of tissue factor expression data from online resources for transcriptomics and proteomics. Tissue factor expression in patient samples was compared in PDAC vs. other cancers (Multi-cancer) and PDAC vs. normal pancreas (Pancreas), as well as between PDAC cell lines vs. cell lines from other cancers (CellLine). Tissue factor protein expression based on immunohistochemistry staining from the Human Protein Atlas is also summarized. **(B)** Patient survival data from The Cancer Genome Atlas (TCGA) pancreatic adenocarcinoma cohort segregated based on tissue factor expression from RNA-Seq. The log-rank P value is displayed.

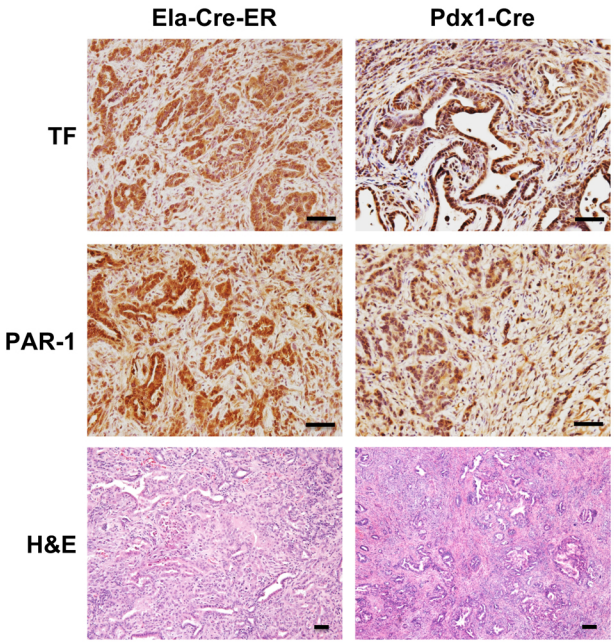

FIGURE S3: *Immunohistochemistry of TF and PAR-1 localization in PDAC from KPC mice.* Staining for TF and PAR-1 of PDAC in pancreata from *KPC* mice. Note that regardless of whether tumorigenesis driven by $Kras^{G12D}/TrP53^{R172H}$ is initiated by *Elastase-Cre-ER* or *Pdx1-Cre*, high levels of PAR-1 and TF are observed in mouse PDAC epithelial lesions. Scale bars: 50 μm.

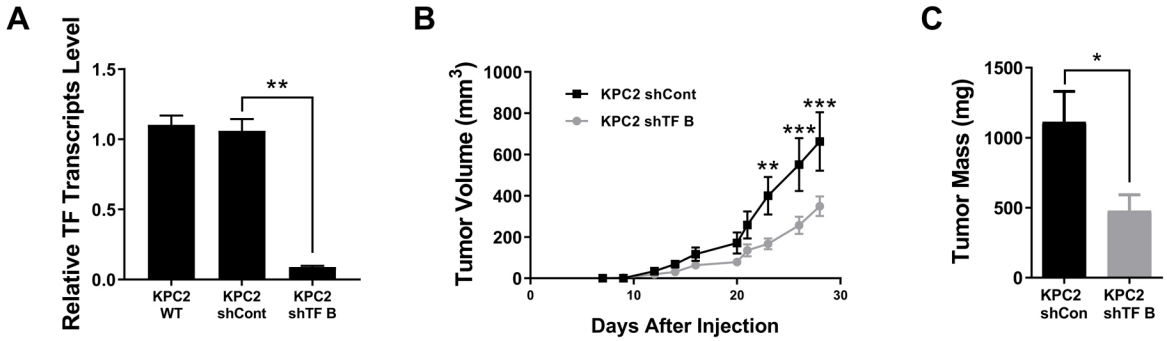

FIGURE S4: *Reduced tumor growth of KPC2 shTF B cells relative to KPC2 shControl cells.* (**A**) RT-qPCR of *TF* transcripts in KPC2 WT, KPC2 shControl and KPC2 shTF B 'knock down' cell lines. (**B,C**) Analysis of tumor growth following subcutaneous injection of KPC2 shControl and KPC2 shTF lines in WT mice (t-test, N=6 mice per group). . * $P < 0.05$; ** $P < 0.01$; *** $P < 0.001$.

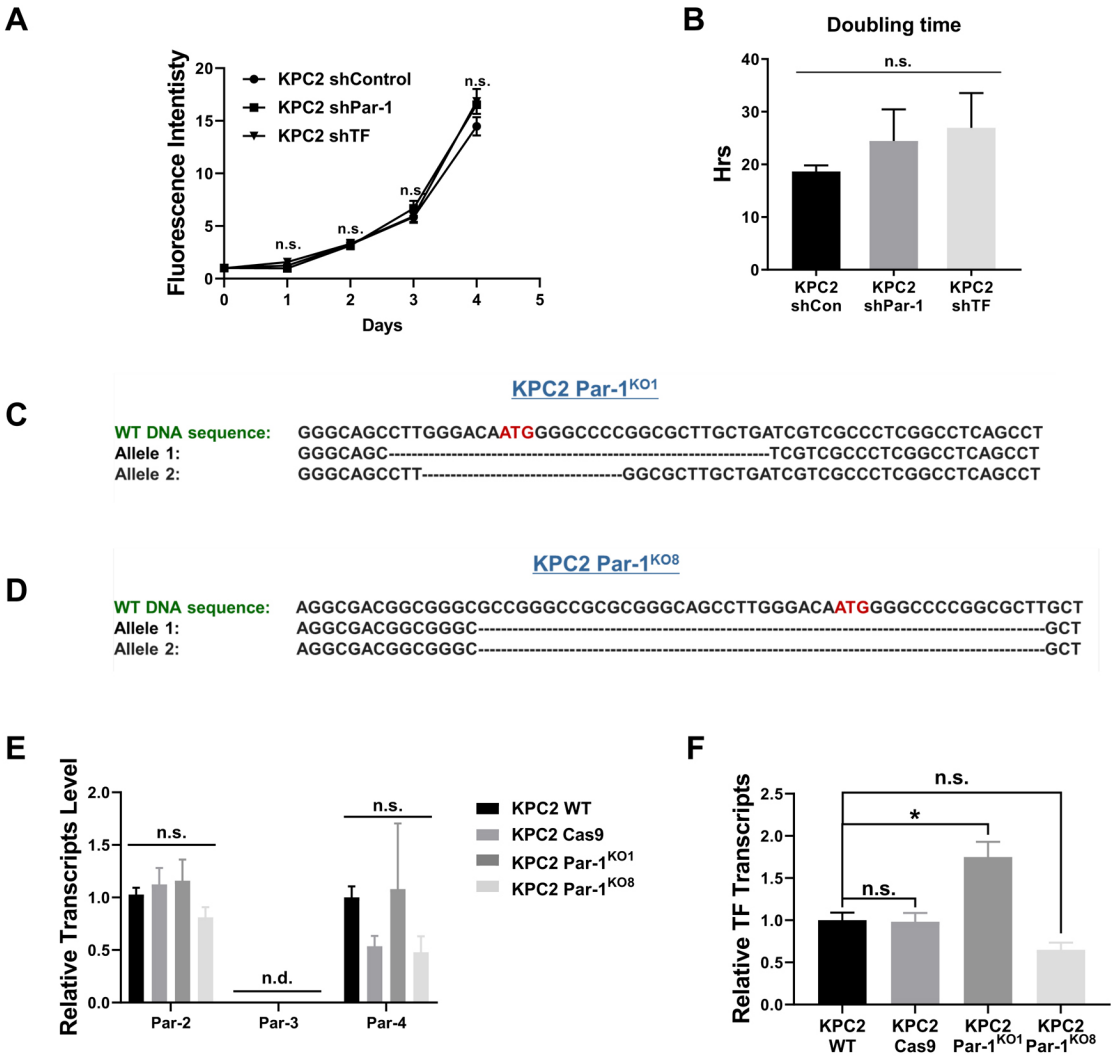

Figure S5: *Analysis of KPC2 shTF, shPar-1, and Par-1^{KO} cell lines in vitro and in vivo.* (**A,B**) Growth curve and doubling times for KPC2 shCont, shPar-1, and shTF cell lines in culture (t-test, N=4). **(C,D)** DNA sequence for KPC2 Par-1^{KO1} and KPC2 Par-1^{KO8} cell lines. The initiation ATG start codon is indicated in red in the DNA sequence. (**E, F**) RT-qPCR analysis of Par receptors and TF for KPC2, KPC2 Cas9, KPC2 Par-1^{KO1}, and KPC2 Par-1^{KO8} cells. * $P < 0.05$; n.s. - not significant; n.d. - not detected.

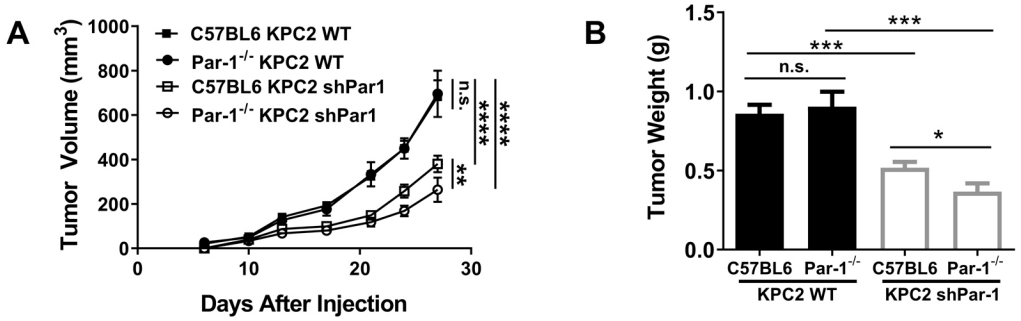

FIGURE S6: *Tumor growth of KPC2 shControl and KPC2 shPAR-1 in C57Bl/6 WT vs. Par-1$^{-/-}$ mice.* **(A,B)** Analysis of tumor volume and final tumor mass following subcutaneous injection of KPC2 shControl cells and KPC2 shPar-1 cells into C57Bl/6 WT and *Par1$^{-/-}$* mice (statistics for tumor volume was calculated using student t-test examining last day tumor volume between groups). * P<0.05; ** P<0.01; *** P<0.001; **** P<0.0001; n.s. - not significant.

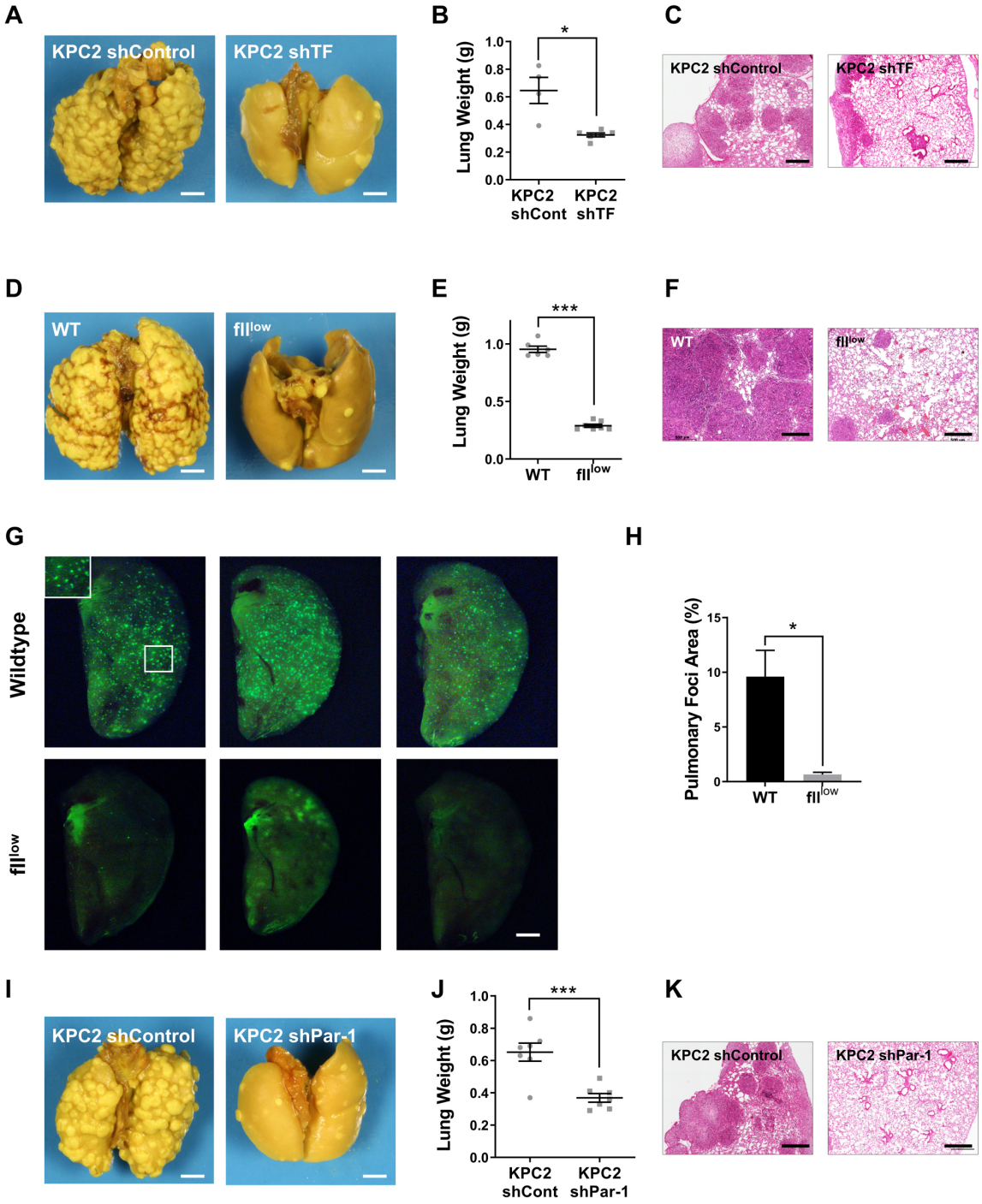

FIGURE S7: *The TF-thrombin-PAR-1 pathway promotes metastatic potential of PDAC cells.* (**A-C**) Analysis of lung metastasis following tail vein injection of KPC2 shControl and KPC2 shTF cells (N=4-6 mice per group). Representative images of lungs harvested 21 days post-injection, total lung weight, and H&E stained lung sections. (**D-F**) Lung metastasis of KPC2 WT cells injected into C57BL/6 WT mice or *fll*^{low} mice (N=6-7 mice per group). Representative images of lungs harvested 21 days post-injection, total lung weight, and H&E stained lung sections. (**G,H**) Lung metastasis of GFP-expressing KPC2 cells tested in WT and *fll*^{low} mice. Cells were injected into the tail vein and then lungs harvested 24 hr post-injection to establish the degree of cell seeding in the lungs (one tailed t-test, N=3). **(I-K)** Metastasis of KPC2 shControl and KPC2 shPar-1 cells in C57Bl/6 mice (N=7 per group). Scale bars: (A,D,I) 2 mm; (C,F,K) 0.5 mm; (G) 1 mm. * $P < 0.05$; *** $P < 0.001$.

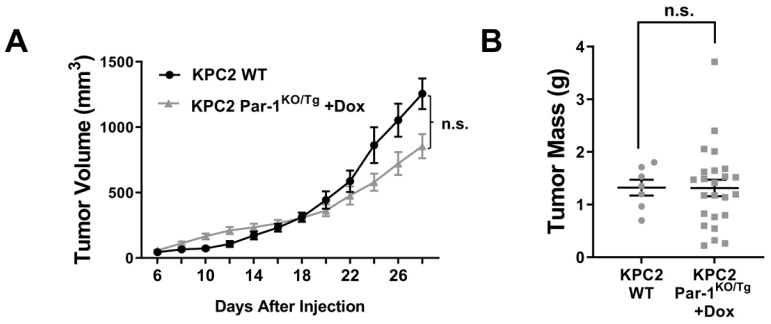

Figure S8: *Analysis of KPC2 WT and Par-1$^{KO/Tg}$ cell lines in vivo.* (**A, B**) Tumor growth and final tumor mass of KPC2 WT and Par-1$^{KO/Tg}$ lines in mice provided Dox. n.s. - not significant.

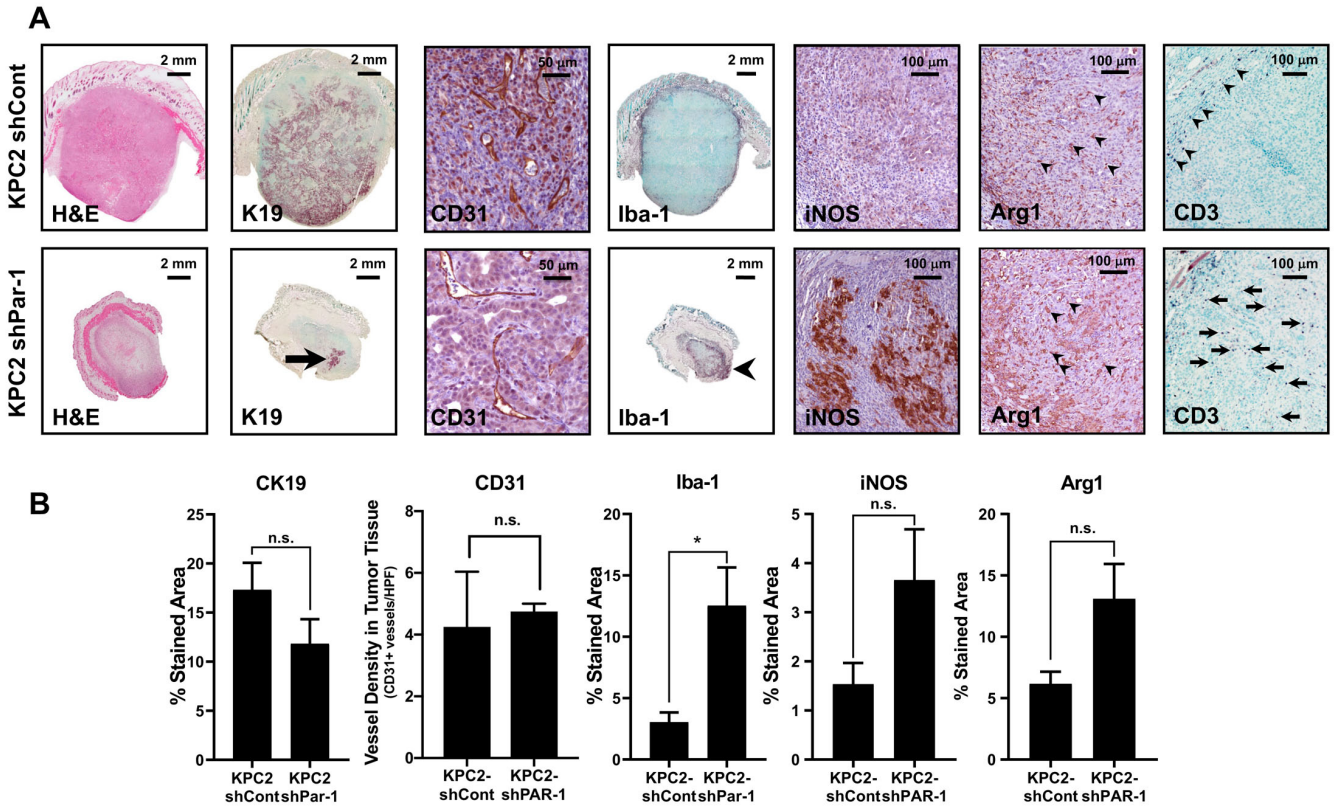

FIGURE S9: *Detection of immune cell infiltrates in KPC2-shControl and KPC2-shPAR-1 tumors.* (**A**) Representative images and (**B**) quantification of staining of tissue sections for H&E, cytokeratin 19 (K19), the endothelial cell marker CD31, the T cell marker CD3, and the macrophage markers Iba-1, iNOS, and Arg1. The sections were generated from isolated tumor tissue 2 weeks following subcutaneous injection of KPC2 shCont and KPC2 shPar-1 cells. Note that large arrows highlight the presence of K19+ KPC2 shPar-1 cells within the overall tumor mass. Small arrowheads denote CD3+ T cells at the tumor periphery whereas small arrows denote CD3+ cell invasion within the tumor. Scale bar: 2 mm, 50 μm or 100μm as noted. * $P < 0.05$. n.s. - not significant.

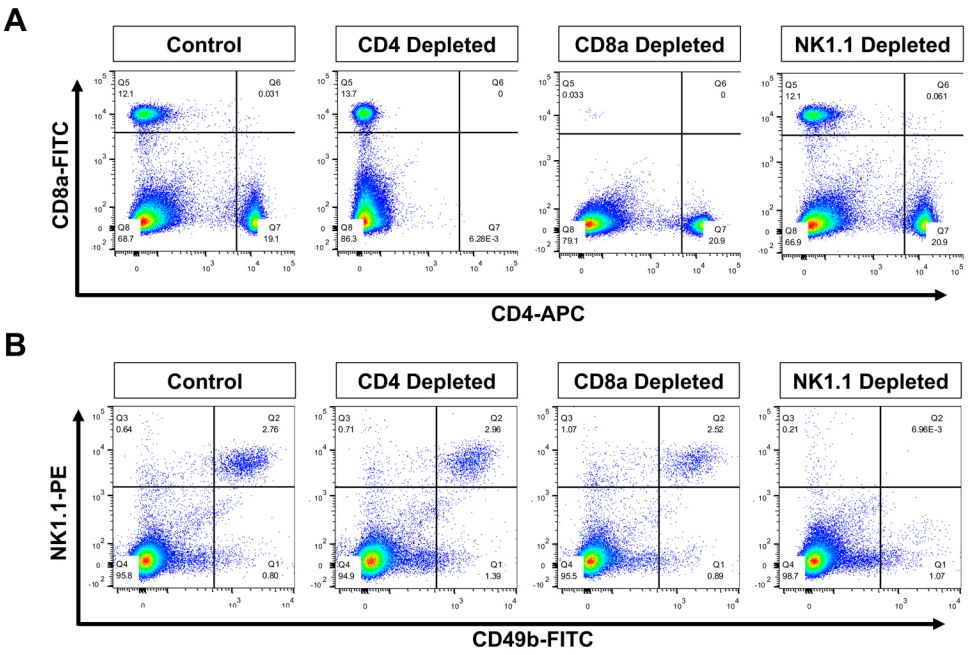

FIGURE S10: *Confirmation of monoclonal antibody mediated in vivo immune cell depletion*. Immune cell subsets were depleted *in vivo* using monoclonal antibodies: CD4 (clone GK1.50), CD8a (clone 2.43), or NK1.1 (clone PK136). Successful depletion was detectable within 18 hours of injection based on flow cytometry of isolated mouse splenocytes and was maintained over the course of the treatment. Representative dot plots from flow cytometry of isolated splenocytes labeled with (**A**) CD8a and CD4 or (**B**) Nk1.1 and CD49b from each treatment group are shown.

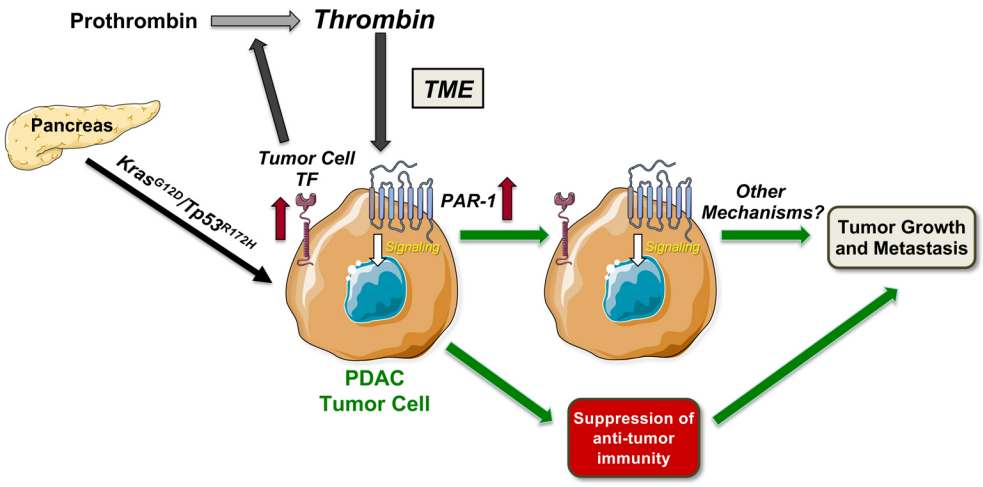

FIGURE S11: *TF-Thrombin-PAR-1 model of PDAC growth.* $KRAS^{G12D}/TP53^{R172H}$-induced transformation leads to upregulation of Tissue Factor (TF) which induces conversion of prothrombin → thrombin in the microenvironment. Thrombin subsequently activates PAR-1 signaling on the tumor cell, initiating downstream events that support primary PDAC tumor growth and metastasis, likely through suppression of anti-tumor immunity.